



An Innovative Equivalent River Channel Method for Integrated Hydrologic-Hydrodynamic Modeling

Yue Yu¹, Chuanhai Wang¹, Gang Chen¹, Hao Wei², Shen Yang¹

¹College of Hydrology and Water Resources, Hohai University, Nanjing 210098, China.

²Shanghai Hydrological Administration, Shanghai, 200232, China

Correspondence to: Gang Chen (gangchen@hhu.edu.cn)

Abstract. To address the lack of river cross-sectional data in hilly regions, this study proposes a novel method that transforms Muskingum parameters (K and X) into Conceptual Equivalent River Channel (CERC). By integrating linear or nonlinear Muskingum parameters with characteristic discharge, roughness, and other relevant inputs, this approach derives simplified yet hydraulically representative cross-sections. Two types of CERC models are introduced: single-layer and dual-layer. The single-layer CERC model includes rectangular, parabolic and triangular cross-sections, while the double-layer CERC builds upon these with an exponential shape. The proposed method was applied to two river reaches in China: the Chenggouwan-Linging reach in the Haihe River Basin and the Huayuankou-Jiahetan reach in the Yellow River Basin. Using previously calibrated and validated Muskingum parameters, the resulting channel geometries were incorporated into a one-dimensional (1-D) hydrodynamic model. Results indicated that CERCs accurately replicated observed hydrographs, and the dual-layer approach improved performance in reaches with strong nonlinear characteristics. Furthermore, the model effectively captured changes in water level and flow velocity, confirming the suitability of CERC for hydrodynamic modeling. A sensitivity analysis examined the impact of variations in roughness (n) affected the Conceptual Equivalent River Channel Cross-sections (CERCXs) and discharge outcomes, demonstrating the robustness of the proposed method. While CERCs simplify the natural complexity of river channels, their parametric framework represents the channel's storage capacity and allows flexible shape selection, enabling accurate simulations of water levels and flow velocities when adjusted to match measured cross-sections. This research provides a practical solution that bridges traditional hydrological and hydrodynamic routing methods in regions with limited data availability, especially in hilly areas.

25 1 Introduction

15

Global climate change, characterized by rising temperatures, shifts in atmospheric circulation, and melting ice sheets, has significantly altered the hydrological cycle (Intergovernmental Panel on Climate Change (IPCC), 2023). Meanwhile, the increasing frequency of extreme rainfall events has intensified flood risk worldwide (Pfahl et al., 2017), underscoring the need for advanced flood modeling in basin management and disaster prevention (Nurbatsina et al., 2025). Accurate flood modelling





not only enhances the reliability of early warning systems but also optimizes flood control operations, thereby mitigating potential damage to both human life and infrastructure (Coletta et al., 2024; Kiesel et al., 2024).

Advancements in computational science and numerical modeling have led to the widespread adoption of one-dimensional (1-D) hydrodynamic models based on the Saint-Venant equations for flood simulation (Liu et al., 2015; Satyaprasad et al., 2023; Ike, 2024). These models provide a more detailed representation of flood processes in both space and time, capturing key variables such as discharge, velocity, and water level. By accurately representing unsteady flow hydrodynamic conditions, 1-D hydrodynamic models offer higher spatial and temporal resolution than traditional hydrological methods, enabling a more precise characterization of flood wave dynamics (Horritt and Bates, 2002; Zhang et al., 2023).

However, to fully leverage the advantages of hydrodynamic modeling, detailed river channel information, especially cross-sectional data, remains essential (Casas et al., 2006). Acquiring these data sets is often costly, time-intensive, making it a major constraint for hydrodynamic simulations. To address this challenge, various studies have explored alternative or supplementary methods for characterizing river channels. For instance, an entropy-based model employing gene expression programming and a maximum entropy framework has been proposed to predict stable channel bank profiles from basic hydraulic parameters (Bonakdari et al., 2020). River cross-sections have also been estimated using a LIDAR-based digital elevation model, with submerged topography reconstructed through an alternative approach validated by 1D/2D HEC-RAS simulations and in situ measurements (Anees et al., 2022). Additionally, the evolving channel morphology of the Barak River has been analyzed using multi-period Landsat imagery (1984–2030), geospatial techniques, and an ARIMA model (Annayat and Sil, 2020). While these approaches can partially compensate for the lack of cross-sectional data, their accuracy is frequently limited by data resolution, inversion algorithms, and region-specific conditions. Moreover, the extensive data processing, filtering, and correction required can be both labor-intensive and technically demanding, especially for mountainous rivers with complex topography.

Conversely, conventional hydrological methods, such as the Muskingum method, remain widely used for flood routing due to their simplicity in parameterization and ease of calibration (Barbetta et al., 2017; Salvati et al., 2023, 2024). Based on the continuity equation and the storage-discharge relationship, the Muskingum method represents channel storage as a combination of prism storage, which corresponds to uniform flow conditions, and wedge storage, accounting for flood wave translation and attenuation (McCarthy, 1939; Cunge, 1969). However, while effective for reproducing discharge hydrographs at an outlet cross-section, the Muskingum method provides limited insight into the internal hydrodynamic conditions within the river channel.

To address this limitation, this study proposes a novel approach for constructing a Conceptual Equivalent River Channel (CERC). Building on previously calibrated Muskingum parameters, whether in a linear or nonlinear form, along with a characteristic discharge Q, channel roughness n, and known reach length L, the channel storage properties are mapped onto a CERC with Conceptual Equivalent River Cross-Sections (CERCXs). To ensure hydraulic representativeness, two CERC models are developed: a single-layer model including rectangular, parabolic, and triangular cross-sections, and a dual-layer model that extends this framework by integrating an exponential profile. This approach provides an innovative method for





transforming Muskingum parameters into input data for one-dimensional hydrodynamic models that solve the Saint-Venant equations. By bridging hydrological and hydrodynamic routing methods, this framework provides reliable simulation results even in the absence of detailed cross-sectional measurements.

The paper is structured as follows: Section 2 introduces the CERC method, Section 3 gives the details of the selected case studies, and Section 4 presents the results obtained from applying the proposed method. Section 5 discusses the effect of key parameter, while Section 6 outlines the limitations and potential application of this approach.

70 2 Methods

2.1 Standard Muskingum Method

The standard Muskingum flood routing model is a widely used hydrological routing method that simulate outflow O_2 as a function of current and previous inflow and outflow, using a set of coefficients (McCarthy, 1939):

$$O_2 = C_0 \cdot I_2 + C_1 \cdot I_1 + C_2 \cdot O_1 , \tag{1}$$

The coefficients C_0 , C_1 and C_2 are based on the Muskingum parameters K and X, as follows:

$$C_0 = \frac{0.5\Delta t - K \cdot X}{K - K \cdot X + 0.5\Delta t},\tag{2}$$

$$C_1 = \frac{0.5\Delta t + K \cdot X}{K - K \cdot X + 0.5\Delta t},\tag{3}$$

$$C_2 = \frac{K - K \cdot X - 0.5\Delta t}{K - K \cdot X + 0.5\Delta t},\tag{4}$$

where Δt is the time step, I and O are inflow and outflow, respectively. The subscript 1 and 2 denote the beginning and end of the time step, while K and X are two key parameters of the Muskingum routing method. K is a storage constant expressing the ratio between storage and discharge in a river reach, while X is a dimensionless weighing factor associated with the characteristic river length, expressed as (Rui et al., 2008):

$$X = \frac{1}{2} - \frac{l}{2L},\tag{5}$$

where l is the characteristic river length and L is the total river reach length.

85 **2.2 Linear and Nonlinear Muskingum Method**

The standard Muskingum method can be categorized into linear and nonlinear formulations, based on whether the routing parameters K and X remain constant or vary with flow conditions. This distinction corresponds to whether the river reach is treated as a single unit or divided into multiple layers with distinct flow characteristics.



90



The linear Muskingum method assumes that the entire river reach is represented by a single set of parameters K and X, simplifying the storage-discharge relationship by treating the reach as a uniform system where storage parameters remain constant regardless of discharge variations. Due to its computational efficiency, the linear Muskingum model is widely used in practical applications where the channel geometry and hydraulic conditions do not change significantly with discharge. In this study, the linear Muskingum parameters are denoted as K_l and K_l respectively.

The nonlinear Muskingum method accounts for flow-dependent variations in storage and routing characteristics by dividing the river reach into multiple layers, each with its own set of Muskingum parameters. This approach is necessary when the river cross-section exhibits significant hydraulic variability across different flow depths. In this study, the Muskingum parameters for the first-layer are denoted as K_{nl1} and X_{nl1} , corresponding to a characteristic discharge Q_1 . Similarly, the second layer's Muskingum parameters are K_{nl2} and X_{nl2} , with an associated characteristic discharge Q_2 .

The nonlinear Muskingum method allows the routing parameters to vary with discharge. In this method, the routing parameters 100 *K* and *X* are not constants but are modeled as linear functions of the characteristic discharge *Q*:

$$K = k_s \cdot Q + k_0, \tag{6}$$

$$X = x_{\rm s} \cdot Q + x_{\rm o},\tag{7}$$

where k_s , k_0 , x_s and x_0 are empirical coefficients derived through calibration.

The characteristic discharge Q is expressed as:

105
$$Q = X \cdot I + (1 - X) \cdot O$$
, (8)

2.3 Derivation of CERC methods from Muskingum Parameters

2.3.1 General Method

To establish a physically based linkage between the Muskingum parameters and river channel properties, Conceptual Equivalent River Channel (CERC) method is proposed. The derivation relies on three fundamental relationships:

Firstly, based on the Manning equation, the flow velocity u is given by:

$$u = \frac{1}{n} R^{\frac{2}{3}} \sqrt{i_0} \,, \tag{9}$$

where u is the flow velocity, n is the roughness coefficient, R is the hydraulic radius, and i_0 is the channel slope.

Wave celerity C is linearly proportional to the flow velocity u via coefficient α , the reach length L is expressed as:

$$L = C \cdot K = K \cdot \alpha \cdot u \,, \tag{10}$$

By combining Eq. (9) with Eq. (10), the reach length L is related to the Muskingum storage constant K as:

$$R^{\frac{2}{3}} \cdot \sqrt{i_0} = \frac{n \cdot L}{\alpha \cdot K},\tag{11}$$





Second, the discharge Q can be expressed as a function of cross-sectional area f(H), hydraulic radius R, and channel slope i_0 , as derived from the Manning formula:

$$Q = \frac{f(H) \cdot R^{\frac{2}{3}}}{n} \cdot \sqrt{i_0} , \qquad (12)$$

Third, the Muskingum parameter X can be related to the spatial variation of flow Q through the characteristic river length l, which is approximated by:

$$l = \frac{Q}{i_0} \cdot \frac{\partial H}{\partial Q},\tag{13}$$

Taking the derivative of Eq.(12) with respect to H, substituting into the expression for l, the following expression for the channel slope i_0 is obtained:

125
$$i_0 = \frac{f(H)}{\left(\frac{1}{2} - X\right) \cdot 2L \cdot \left(f'(H) + \frac{2}{3} f(H) \cdot R^{-1} \cdot R'\right)},$$
 (14)

Thus, Eqs. (11), (12), and (14) establish the relationship between Muskingum parameters K and X and the CERC. The full derivation of these expressions, including partial derivatives and substitutions, is provided in Appendix A.1.

2.3.2 Adjustment of Wave-to-Flow Velocity Conversion Coefficient

To further refine the calculation of the wave-to-flow velocity conversion coefficient α , a constant value is no longer used. 130 Instead, α is dynamically adjusted according to the proposed CERCX. The wave celerity C is given as follows:

$$C = \frac{dQ}{dA} = u \left(1 + \frac{A}{v} \frac{du}{dA} \right), \tag{15}$$

Thus, the adjusted α is expressed as:

$$\alpha = 1 + \frac{A}{u} \frac{du}{dA} = 1 + \frac{2}{3} R' \,, \tag{16}$$

Detailed derivation is provided in Appendix A.2.

135 2.3.3 Single-Layer CERC Method

Based on the general formulas derived in Section 2.3.1, a single-layer Conceptual Equivalent River Channel (CERC) can be constructed using linear Muskingum parameters K_l and X_l . Various cross-sectional shapes can be considered by specifying their corresponding cross-sectional area function f(H). In this study, three typical geometries are examined: rectangular, parabolic, and triangular.

140 For Rectangular-shaped CERCX:

$$f(H_r) = B_r \cdot H_r \,, \tag{17}$$



155



For Parabolic-shaped CERCX:

$$f(H_p) = \int_0^{H_p} B_p dh_p = \frac{2}{3} \beta H_p^{\frac{3}{2}}, \tag{18}$$

For Triangular-shaped CERCX:

$$45 \quad f(H_t) = 0.5H_t \cdot B_t \,, \tag{19}$$

Given these expressions, other hydraulic properties, including the hydraulic radius R, the channel slope i_0 , the top width B, the bankfull depth H and the adjusted coefficient α can be determined by substituting into Eqs. (11), (12), (14), and (16) introduced earlier. Detailed derivations are provided in Appendix A.3. This paper focuses on the formulas for parabolic, rectangular and triangular CERCX. Other cross-sectional geometries, such as trapezoidal, can be derived using the same principles but are not discussed in detail here.

2.3.4 Dual-Layer CERC Method

For compound channels, a dual-layer CERC method is introduced based on the single-layer CERC formulas proposed in Section 2.3.3. The schematic diagram of the dual-layer CERCX is shown in Fig.1. In this approach, the actual compound channel cross-section, which exhibits nonlinear hydraulic characteristics, is approximated by two layers of CERCX.

Muskingum parameters of the second layer: K_{nl2} , X_{nl2} , Q_2 BMuskingum parameters of the first layer: K_{nl1} , X_{nl1} , Q_1 B_1 H_1

Figure 1: Diagram of Dual-Layer CERCX

For each layer, the characteristic discharge Q and Muskingum parameters K and X should be determined accordingly. The Muskingum parameters for the first-layer are denoted as K_{nl1} and X_{nl1} , with an associated characteristic discharge of Q_1 . Similarly, the second layer's Muskingum parameters are K_{nl2} and X_{nl2} , corresponding to characteristic discharge of Q_2 .

Geometrically, the top width of the first-layer CERCX, B_1 , equals the bottom width of the second-layer CERCX, while B represents the top width of the dual-layer CERCX. The bankfull depths of the first and second layers are denoted as H_1 and H_2 , respectively, while the total bankfull depth of the dual-layer CERCX, H, is given by $H = H_1 + H_2$.





When the second-layer CERCX is approximated using an exponential shape, the top width of the cross-section is expressed as:

$$165 \quad B_e = b \cdot H_2^{\ a} + B_1 \,, \tag{20}$$

Accordingly, the corresponding cross-sectional area $F(H_2)$ and the derivative of the hydraulic radius $R'(H_2)$ are given by:

$$F(H_2) = \int_0^{H_2} B_e \, dh = \frac{b}{a+1} H_2^{a+1} + B_1 \cdot H_2 + A_1 \,, \tag{21}$$

where a and b are the cross-sectional shape parameters.

Given the known parameters K_{nl2} , X_{nl2} , and Q_2 , the unknowns for the second layer, including a, b and H_2 can be derived by applying the general formulas introduced in Section 2.3.1. In addition, the adjusted coefficient α_2 for the second layer can be determined by substituting the derivative of the hydraulic radius $R'(H_2)$ into Eq. (16). Detailed derivation is provided in Appendix A.4.

Similarly, for a parabolic approximation of the second-layer CERCX, the top width of dual-layer cross-section is given by $B_p = b\sqrt{H_2} + a + B_1$. For a trapezoidal approximation, the top width is expressed as $B_t = bH_2 + a + B_1$. Since the shape parameter a represents a discontinuity in the cross-section of the second layer, the parabolic and trapezoidal approximations for the second-layer CERCX lead to unsolvable conditions. Therefore, the current approach defines the second-layer CERCX using an exponential shape, ensuring continuity and consistency in the hydraulic representation.

2.4 Evaluation Measures

185

To assess the storage ability of the proposed CERC approach to simulate discharge in a 1-D hydrodynamic model, three evaluation metrics were employed: Root Mean Squared Error (*RMSE*), Nash–Sutcliffe coefficient (*NS*), and Error Percentage of Discharge (*EPQ*).

The Root Mean Squared Error (*RMSE*) measures the deviation between simulated and observed discharge. Its unit is consistent with discharge, expressed in m³/s. A smaller *RMSE* value indicates a smaller simulation error. The Nash–Sutcliffe coefficient (*NS*) evaluates the goodness of fit between simulated and observed discharge, ranging from 0 to 1. An *NS* value closer to 1 indicates higher simulation accuracy.

The RMSE and the NS are calculated using the following equations, respectively:

$$RMSE = \sqrt{\frac{1}{N} \sum_{i=1}^{N} [Q_{sim}(i) - Q_{0bs}(i)]^2},$$
(22)

$$NS = 1 - \frac{\sum_{i=1}^{N} [Q_{sim}(i) - Q_{0bs}(i)]^2}{\sum_{i=1}^{N} [Q_{obs}(i) - \bar{Q}_{obs}(i)]^2},$$
(23)

The *EPQ* quantifies the discrepancy between simulated and observed peak discharge. A value closer to 0 indicates a smaller error in peak discharge estimation. *EPQ* metric is defined as:





$$EPQ = \frac{Q_{0bs_max} - Q_{sim_max}}{Q_{obs_max}} * 100\%, \qquad (24)$$

3 Case Studies

195

205

To evaluate the performance of the proposed CERC approach under varying flow and channel conditions within a 1-D hydrodynamic model, two river reaches in China with distinct hydrological and morphological characteristics were selected (Fig. 2): (1) The Chenggouwan–Linqing reach of the Haihe River Basin; (2) The Huayuankou–Jiahetan reach of the Yellow Piver Basin

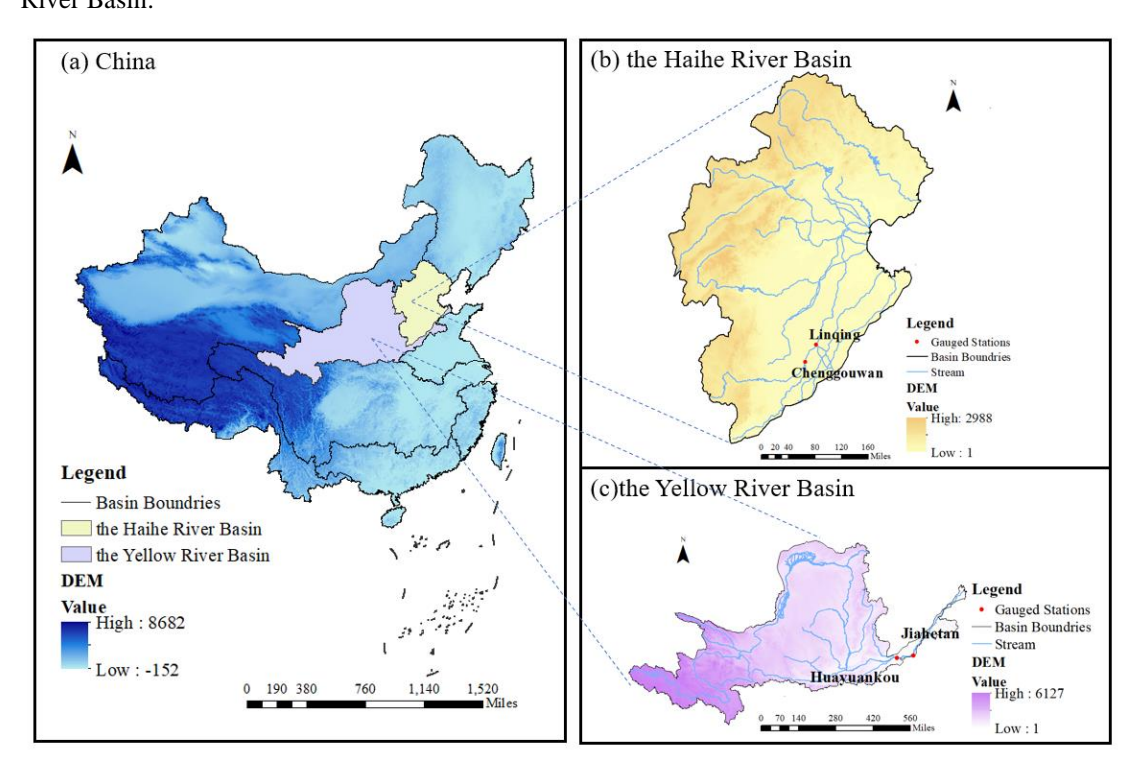


Figure 2: Study Area of the Selected River Reaches

3.1 Chenggouwan-Linqing Reach

The South Canal, located in the southern part of Hebei Province, China, is the longest river in the Haihe River system. The selected reach, extending from Chenggouwan Station to Linqing Station, has a total length of 83.8 km. A flood event lasting 336 hours was selected for analysis.

For hydrodynamic simulations, the river channel was generalized as a uniform channel segment with a length of 83.8 km. The Manning's roughness coefficient n was set to 0.02. The single-layer equivalent channel method was employed to approximate the cross-sectional geometry of the reach. Hydrodynamic simulations solving the Saint-Venant equations were performed



225



using the CERC. The corresponding parameters are provided in Table 1. The Muskingum parameters K and X were adopted from He and Zhang (1998), which applied a least squares approach for parameter estimation. The discharge parameter Q was set to 600 m³/s, representing a characteristic value based on the inflow process. This value primarily serves to characterize the morphology of the CERCX under specific peak discharge conditions.

210 3.2 Huayuankou-Jiahetan Reach

The Huayuankou–Jiahetan reach, located in the lower reaches of the Yellow River, spans a total length of 105.4 km. The Yellow River is the second-longest river in China, characterized by substantial sediment transport due to its passage through the Loess Plateau. Consequently, the lower Yellow River exhibits a compound cross-sectional profile with pronounced nonlinear characteristics. A flood event lasting 116 hours was selected for analysis.

The river channel was simplified as a continuous reach of 105.4 km, with a roughness coefficient *n* set to 0.02. Hydrodynamic simulations were conducted using both the single-layer and dual-layer equivalent channel methods, with the relevant parameters summarized in Tab.1. For the single-layer case, Muskingum parameters were calibrated using a stepwise routing approach over sub-reaches, whereas for the dual-layer case, a nonlinear Muskingum method was employed with iterative parameter adjustment based on observed hydrographs.

Table 1: Parameters for CERC in Two Reaches

Reach	CERC Method	n	K	X	$Q(m^3/s)$	
Chenggouwan-Linqing	Single-Layer	0.02	13.05	-0.2716	600	
	Single-Layer	0.02	12.6	-0.7	14800	
Huayuankou-Jiahetan	Dual-Layer (the first-layer)	0.02	15	-0.1	5000	
	Dual-Layer (the second-layer)	0.02	13.5	-1	20000	

Based on the derived CERCX, the depth-discharge relationship at downstream cross-section was determined using Eq.(9), while the velocity-discharge relationship was expressed as $u = \frac{Q}{A}$. In the 1-D hydrodynamic model, numerical simulations were performed using the observed discharge at the upstream boundary. At the downstream boundary, the depth-discharge relationship was prescribed as the boundary condition.





4 Results

4.1 CERCX

4.1.1 Chenggouwan-Linqing Reach

For the Chenggouwan–Linqing reach, simulations were performed using the linear Muskingum parameters with three different cross-sectional shapes: rectangular, parabolic, and triangular. The corresponding configurations are illustrated in Fig.3, with their parameters detailed in Tab.2.

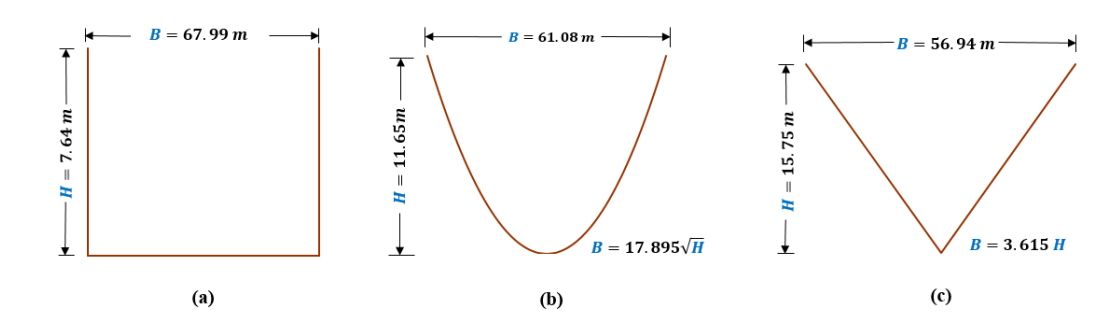


Figure 3: Schematic Diagrams of Single-Layer CERCX for Chenggouwan–Linqing Reach: (a) Rectangular, (b) Parabolic, and (c) Triangular

235 Table 2: Detailed CERCX Parameters for Chenggouwan-Linqing and Huayuankou-Jiahetan Reaches

Reach	CERC Method	Shape	<i>i</i> ₀ (‰)	B(m)	H(m)	<i>B</i> ₁ (m)	<i>H</i> ₁ (m)	<i>H</i> ₂ (m)	β	γ	а	b
Chenggouw		Rectangular	0.36	67.99	7.64	-	-	-	-	-	-	-
an–Linqing	Single-Layer	Parabolic	0.42	61.08	11.65	-	-	-	17.9	-	-	-
		Triangular	0.46	56.94	15.75	-	-	-	-	3.62	-	-
		Rectangular	0.29	869.08	12.08	-	-	-	-	-	-	-
	Single-Layer	Parabolic	0.35	722.08	19.10	-	-	-	165.2	-	-	-
Huayuankou		Triangular	0.39	644.74	26.34	-	-	-	-	24.48	-	-
-Jiahetan		Rectangular	0.37	795.60	26.15	546.07	7.73	18.42	-	-	2.76	0.08
	Dual-Layer	Parabolic	0.45	653.54	32.09	453.85	12.22	19.87	129.8	-	3.89	0.00
		Triangular	0.50	608.79	37.69	405.26	16.86	20.83	-	24.04	4.36	0.00

Note: For the dual-layer CERC method, the listed cross-sectional shapes refer to the first layer.





4.1.2 Huayuankou-Jiahetan Reach

For the Huayuankou–Jiahetan reach, both the single-layer and dual-layer CERC methods were employed to approximate the cross-section. In the single-layer approach, the cross-section was approximated by rectangular, parabolic, and triangular shapes. In the dual-layer approach, the first-layer was approximated using three distinct shapes. Figure 4 provides a schematic representation of these configurations, while the associated parameters detailed in Tab.2.

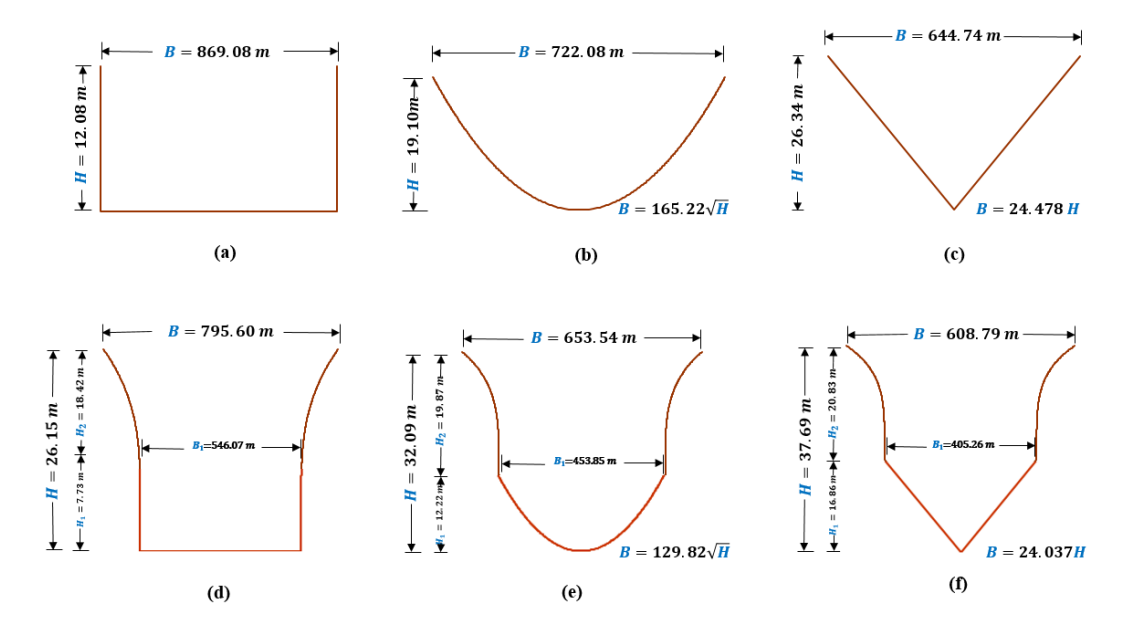


Figure 4: Schematic Diagrams of Single-Layer and Dual-Layer CERCX for Huayuankou-Jiahetan Reach: (a)-(c) Single-Layer CERCX (Rectangular, Parabolic, Triangular); (d)-(f) Dual-Layer CERCX with Rectangular, Parabolic, and Triangular First-layer

245 **4.2 Discharge Simulation**

250

255

By synthesizing the discharge results from both the Chenggouwan–Linqing and Huayuankou–Jiahetan reaches (Fig.5), the proposed CERC method effectively replicates the outflow hydrographs and captures the channel's storage capacity under varied hydrological conditions. In the Chenggouwan–Linqing reach, all three cross-sectional approximations demonstrated excellent agreement with observed data at Linqing Station, achieving an *NS* of 0.99, an *RMSE* below 12.45 m³/s (around 2.7% of the average discharge), and an *EPQ* consistently under 0.3%. These results are summarized in Tab.3.

In the Huayuankou–Jiahetan reach, where channel conditions exhibit stronger nonlinearity, both single-layer and dual-layer CERC approaches showed high fidelity in reproducing observed outflows. Model performance metrics achieved $NS \ge 0.97$, with RMSE values constrained to a maximum of 822.92 m³/s (approximately 9.9% of the average discharge). Notably, under peak flow conditions, the dual-layer approach demonstrated superior performance, achieving an average EPQ of 1.36%, representing a 4% absolute reduction compared to the single-layer approach (average EPQ = 5.36%). This improvement





highlights the dual-layer method's ability to better capture complex nonlinear storage dynamics. However, while the single-layer approach exhibited lower accuracy in peak flow estimation, it provided a more precise representation of peak timing, aligning more closely with observed data. In practical applications, when only the calibrated linear Muskingum parameters are available, the single-layer CERC method remains a viable and reliable option.

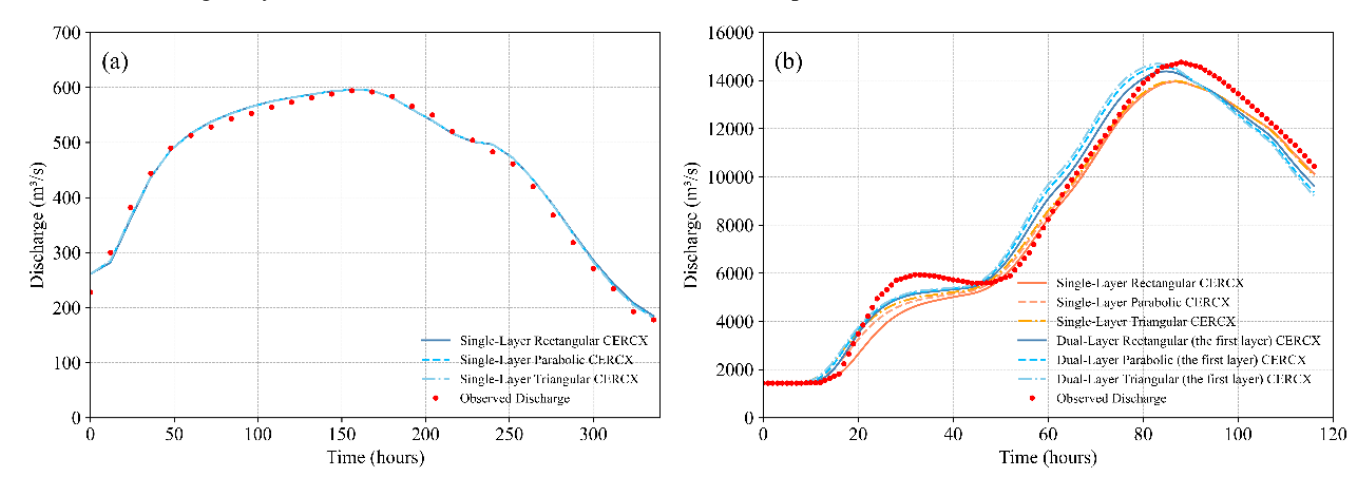


Figure 5: Observed and Simulated Discharge Hydrograph at (a) Linqing Station and (b) Jiahetan Station

Table 3: Performance Metrics (RMSE, NS, EPQ) for Discharge Results

Reach	CERC Method	Shape	$RMSE(m^3/s)$	NS	EPQ (%)
		Rectangular		0.99	0.29
Chenggouwan-Linqing	Single-Layer	Parabolic	11.61	0.99	0.29
		Triangular	12.45 0.99 0 11.61 0.99 0 11.46 0.99 0 638.00 0.98 5 533.59 0.99 5 512.52 0.99 5 564.67 0.98 2 723.19 0.97 1	0.30	
		Rectangular	638.00	0.98	5.49
	Single-Layer	Parabolic	533.59	0.99	5.36
Huarmankan Lahatan		Triangular	512.52	0.99	5.23
Huayuankou-Jiahetan		Rectangular	564.67	0.98	2.55
	Dual-Layer	Parabolic	723.19	0.97	1.12
		Triangular	822.92	0.97	0.42

Note: For the dual-layer CERC method, the listed cross-sectional shapes refer to the first layer.





4.3 Water Level Simulation

Figure 6 shows the measured channel cross-section at Chenggouwan Station, which exhibits an irregular geometry with a main channel width of 52.78 m. The proposed CERCX adopts an idealized approach, assuming a high degree of symmetry in channel geometries to establish a conceptualized schematization of cross-sectional dimensions. Notably, the single-layer rectangular CERCX closely aligns with the morphology of the measured cross-section.

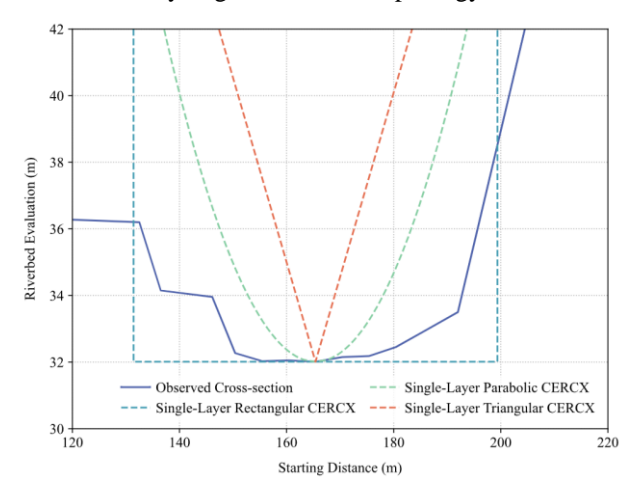


Figure 6: Comparison of the Measured Cross-Section with the Single-Layer CERCX at Chenggouwan Station

By integrating CERCXs into the 1-D hydrodynamic model, water levels were simulated. A comparative analysis of three CERX representations (single-layer rectangular, parabolic, and triangular cross-sections) revealed distinct performances in Chenggouwan–Linqing reach (Fig.7). The single-layer rectangular CERCX method exhibited the best agreement with observed water levels at Linqing Station, with a maximum relative error of 4.5% and minimum error of 0.1%.

This performance hierarchy (rectangular > parabolic > triangular) correlates strongly with the morphological similarity between the conceptualized geometry and the measured cross-section. Theoretically, improved simulation accuracy is expected when employing parabolic or triangular CERCXs in reaches with corresponding geometric characteristics. Conversely, this correlation implies that hydraulic inversion using observed water level data could enable probabilistic estimation of river channel cross-sectional geometry within data-scarce reaches.

280

270

275





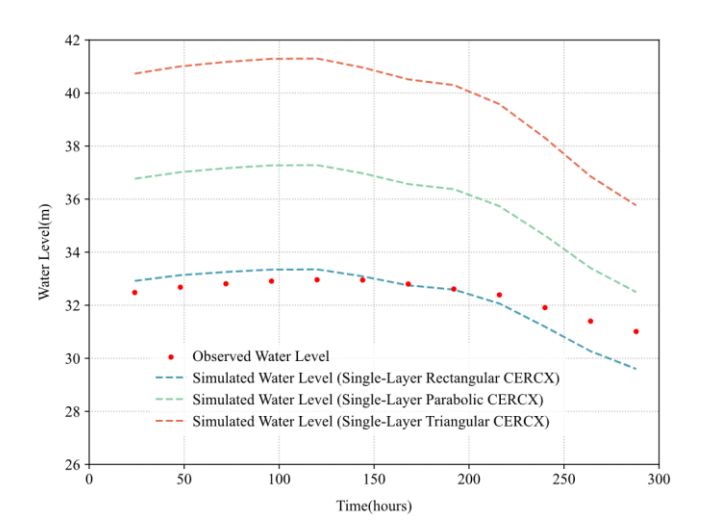


Figure 7: Comparison of Observed and Simulated Water Level at the Linqing Station

4.4 Flow Velocity Simulation

285

290

Beyond water level estimation, the 1D hydrodynamic model enables flow velocity simulation at any cross-section and time point. Figure 8 illustrates the temporal evolution of velocity along eight cross-sections (0 km, 12.57 km, 25.14 km, 37.71 km, 50.28 km, 62.85 km, 75.42 km, and 83.8 km) along the Chenggouwan–Linqing reach using single-layer rectangular CERCXs. Notably, at the 48-hour mark, velocity values at all sections converged, marking a clear transition in the flow process. Prior to this point, velocities gradually increased as the discharge wave propagated downstream. Thereafter, velocities began to decline due to reduced inflows.

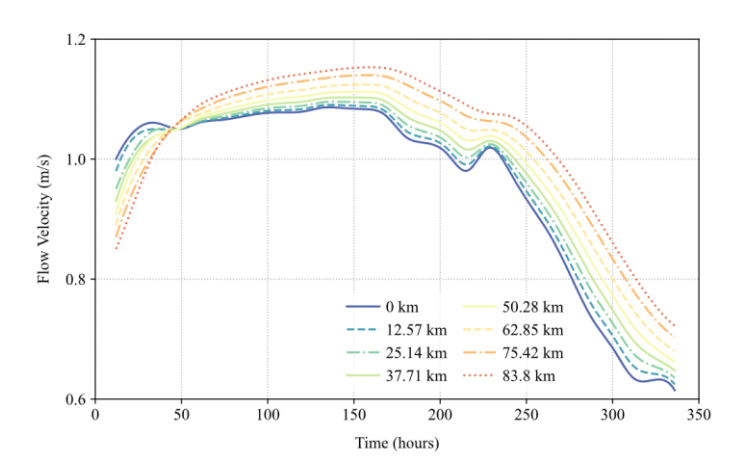


Figure 8: Simulated Flow Velocities at Multiple Cross-Sections of the Chenggouwan-Linqing Reach (Single-Layer Rectangular CERC)



295

300

310

315

320



5 Parameter Sensitivity Analysis

The CERC method proposed in this study, based on Muskingum parameters, transforms parameters (K, X, Q, n, L) into equivalent river channels (i_0, B, H) that reflect channel storage properties. Since Muskingum parameters K, X and Q have been calibrated and validated, and the river length L is a fixed, known value, the analysis focuses on the sensitivity of the roughness coefficient n. Additionally, since the method relies on pre-calibrated Muskingum parameters, any uncertainties in these parameters could impact the derived channel characteristics, highlighting the importance of proper validation.

In the two case studies presented above, a default river roughness coefficient of 0.02 was used. However, in real river channels, the value of n is influenced by factors such as bed morphology and vegetation cover, resulting in significant spatial variability. According to Niu et al (2024), the roughness coefficient in the Huayuankou-Jiahetan reach varies between 0.01 and 0.06. To quantify the impact of roughness, the Huayuankou-Jiahetan reach was used as a case study, with n varied in increments of 0.01 (n = 0.01, 0.02, ..., 0.06).

5.1 Morphology of Equivalent River Channel

305 The effect of varying n on the morphology of single-layer and dual-layer CERCX models is shown in Fig. 9 and Fig. 10.

5.1.1 Average Slope of River Channel i_0

For both the single-layer and dual-layer CERC models, i_0 increased as the roughness coefficient n increased. In the single-layer CERC model, the variation trend of i_0 remained consistent across different cross-sectional shapes. Similarly, in the dual-layer CERC model, i_0 increased with n; however, both the magnitude and variability of i_0 were slightly higher than those observed in the single-layer model.

5.1.2 Width of Cross-Section B, B_1

The cross-section width decreased as n increased in both single-layer and dual-layer CERC models, although the rate of decrease varied. In the single-layer model, the width B of the rectangular CERCX was most sensitive to changes in roughness, while the triangular CERCX was least affected. In the dual-layer model, both the bottom layer width B_1 and the total channel width B exhibited a significant decrease with increasing n, particularly for lower roughness values (0.01 $\leq n \leq$ 0.03). However, with the rate of decrease slowed for higher roughness values (0.04 $\leq n \leq$ 0.06).

5.1.3 Depth of Cross-Section H, H₁, H₂

The depth of cross-section increased with increasing roughness n for both conceptualization methods. In the single-layer CERC model, the increase in depth H was most pronounced for the triangular CERCX and least for the rectangular CERCX. A similar trend was observed in the dual-layer model, where the increase in depth H, H_1 , and H_2 was greatest when the first-layer had a triangular shape, followed by the parabolic CERCX, with the rectangular first-layer exhibiting the smallest increase.





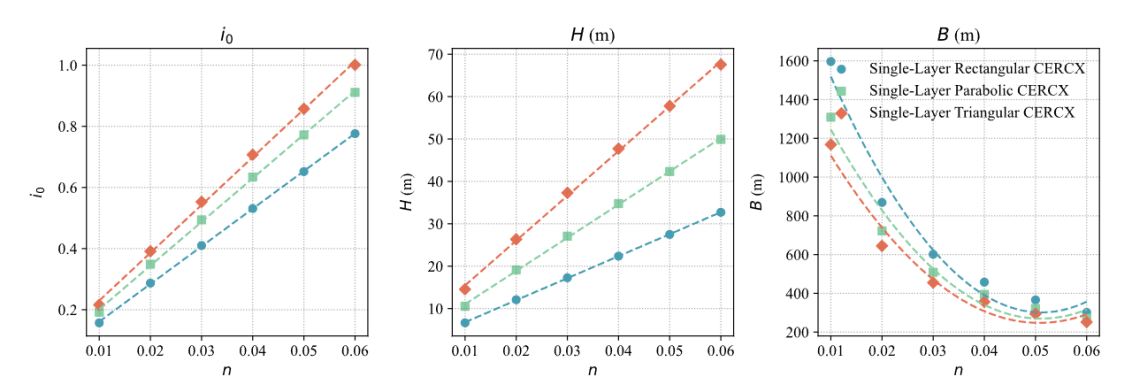


Figure 9: Effect of Different Roughness Coefficients (n) on the Morphology of Single-Layer CERCX for Huayuankou-Jiahetan Reach

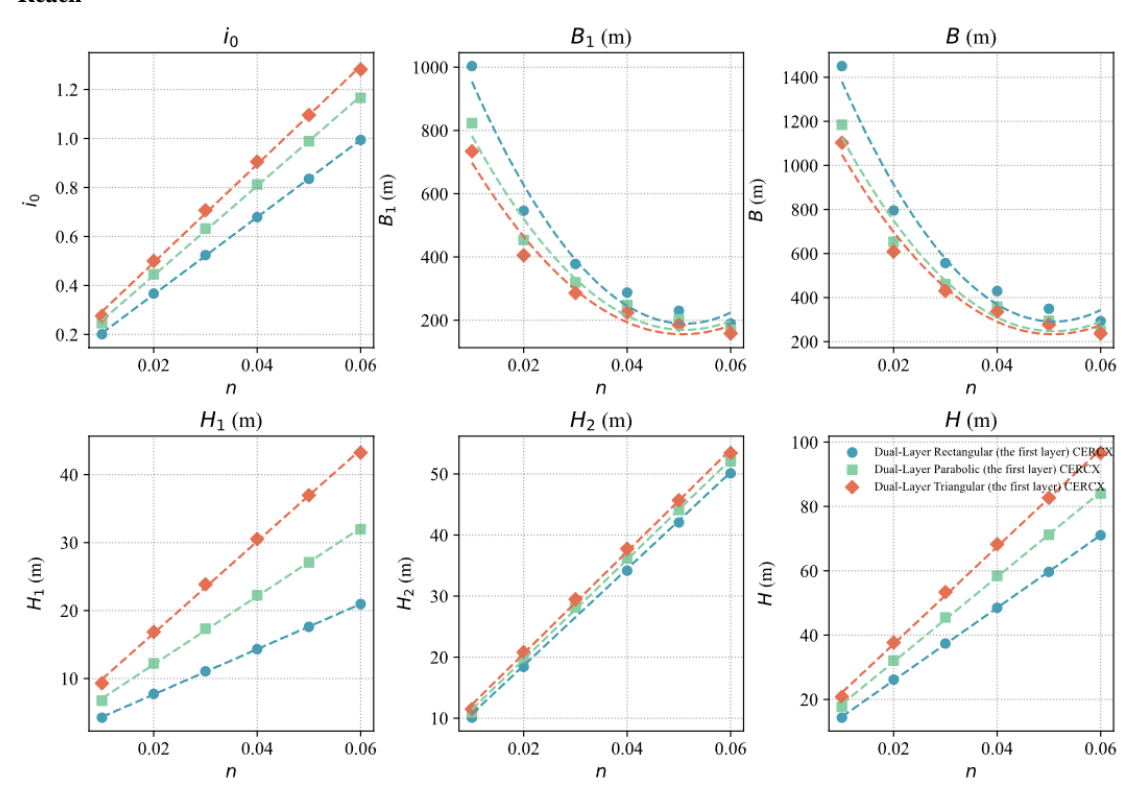


Figure 10: Effect of Different Roughness Coefficients (n) on the Morphology of Dual-Layer CERCX for Huayuankou-Jiahetan Reach

5.2 Simulation Results in 1-D Hydrodynamic Model

The performance metrics (*RMSE*, *NS*, and *EPQ*) for the single-layer and dual-layer CERC models under different roughness coefficients (*n*) in a 1-D hydrodynamic model are presented in Tab.4 and Tab.5.





As roughness increased, both models showed a decreasing trend in *RMSE*. Among the different cross-sectional shapes, the *RMSE* for the triangular CERCX remained the lowest, followed by the parabolic cross-section, while the rectangular CERCX had a relatively higher *RMSE*, though the overall differences were not significant. For both single-layer and dual-layer CERC models, the *NS* value remained above 0.97, indicating a high degree of agreement between the simulated discharge and observed discharge across varying roughness conditions. Similarly, the *EPQ* remained low for both models and exhibited a decreasing trend as roughness increased.

Table 4: Performance Metrics (RMSE, NS, EPQ) for Single-Layer CERC at Different Roughness Coefficients (n) in a 1D Hydrodynamic Model for Huayuankou-Jiahetan Reach

20	RMSE (m ³ /s)			NS			<i>EPQ</i> (%)		
n	rectangular	parabolic	triangular	rectangular	parabolic	triangular	rectangular	parabolic	triangular
0.01	642.86	536.02	517.65	0.98	0.99	0.99	5.54	5.38	5.25
0.02	638.00	533.59	512.52	0.98	0.99	0.99	5.49	5.36	5.23
0.03	628.48	532.56	510.25	0.98	0.99	0.99	5.39	5.35	5.22
0.04	616.37	530.32	507.88	0.98	0.99	0.99	5.25	5.31	5.21
0.05	602.56	526.60	505.64	0.98	0.99	0.99	5.09	5.25	5.21
0.06	587.86	521.78	503.46	0.98	0.99	0.99	4.92	5.16	5.21

340 Table 5: Performance Metrics (RMSE, NS, EPQ) for Dual-Layer CERC at Different Roughness Coefficients (n) in a 1D Hydrodynamic Model for Huayuankou-Jiahetan Reach

		RMSE (m ³ /	s)		NS		<i>EPQ</i> (%)			
n	rectangular	parabolic	triangular	rectangular	parabolic	triangular	rectangular	parabolic	triangular	
0.01	563.44	727.09	827.72	0.98	0.97	0.97	2.63	1.11	0.40	
0.02	564.67	723.19	822.92	0.98	0.97	0.97	2.55	1.12	0.42	
0.03	570.65	723.07	820.02	0.98	0.97	0.97	2.43	1.11	0.42	
0.04	579.57	725.19	816.00	0.98	0.97	0.97	2.29	1.07	0.42	
0.05	591.13	730.05	810.02	0.98	0.97	0.97	2.12	1.01	0.40	
0.06	605.01	736.99	801.38	0.98	0.97	0.97	1.93	0.93	0.39	

Note: The listed cross-sectional shapes refer to the first-layer of the dual-layer CERC



345

350

355

360



6 Discussion and conclusion

This study presents a novel method to addressing the lack of river channel data in hydrological and hydrodynamic modeling by transforming Muskingum K and X parameters, along with other readily available parameters such as characteristic discharge Q, roughness coefficient n, and wave-to-flow velocity conversion coefficient α , into formulas for Conceptual Equivalent River Channel (CERC). Two types of CERC models are introduced: single-layer and dual-layer. The single-layer CERC model includes rectangular, parabolic and triangle cross-sections, while the double-layer CERC builds upon these with an exponential shape. This method enables the estimation of key hydraulic characteristics, including channel cross-section top width B, channel slope i_0 , and bankfull depth H, providing a practical approach for integrating hydrological methods into hydrodynamic simulations, particularly in data-scarce and hilly regions.

Despite its effectiveness, the proposed method has certain limitations. The conceptualization of cross-sectional shapes (rectangular, parabolic, and triangular) may not fully capture the complexities of real-world river morphology, especially in highly irregular or meandering channels. It is important to note that the equivalent river channel is primarily designed to reflect the storage capacity of a river reach rather than precisely match its actual cross-sectional profile. While the method provides a practical approach for integrating hydrological and hydrodynamic models, it does not aim to replicate fine-scale geometric details of individual river cross-section. However, the inclusion for different conceptualized cross-sectional shapes provided in this study allow for the selection of the most appropriate and representative equivalent shape when at least one cross-sectional profile is available. By incorporating actual cross-sectional data, the method can be further refined to improve not only discharge predictions but also water level and flow velocity estimates, enhancing its applicability in hydrodynamic modeling.

Overall, this study provides a computationally efficient and practical framework for hydrodynamic modeling in data-scarce regions, bridging the gap between hydrological and hydrodynamic approaches. Future work will further explore its application in more complex hydrologic—hydrodynamic interaction systems involving lateral inflows and backwater effects.



370



CRediT authorship contribution statement

Yue Yu: Conceptualization, Methodology, Results analysis, Visualization, and Writing – original draft and revision. Chuanhai Wang: Conceptualization, Methodology – review. Gang Chen: Supervision, Conceptualization, Methodology, and - review and editing. Hao Wei: Writing – review and editing. Shen Yang: Writing – review and editing.

Software availability

The distributed-framework basin modeling system Taihu Basin Model (TBM) was written in C++ and compiled with Microsoft Visual Studio. It is available for trial download application at http://www.digitalwatershed.cn/down.aspx, only a Chinese version is currently available.

375 Declaration of competing interest

The authors declare that they have no known competing financial interests or personal relationships that could have appeared to influence the work reported in this paper.

Acknowledgments

This research was financially supported by the National Natural Science Foundation of China (U2240209), and Hydraulic Science and Technology Program of Jiangsu Province (2022003).





Appendix A. Detailed Derivation of the CERC Method

This appendix presents the complete mathematical derivation of the Conceptual Equivalent River Channel (CERC) method based on Muskingum parameters, including both single-layer, dual-layer and adjusted α formulations.

A.1 General Method

The Manning formula for flow velocity u is given as follows:

$$u = \frac{1}{n} R^{\frac{2}{3}} \sqrt{i_0} \,, \tag{A1}$$

where u is the velocity, n is the roughness coefficient, R is the hydraulic radius and i_0 is the slope.

390 Wave celerity *C* is related to flow velocity by:

$$C = \alpha \cdot u \Rightarrow L = C \cdot K = K \cdot \alpha \cdot u , \tag{A2}$$

Substituting Eq. (A1) into Eq. (A2) yields:

$$R^{\frac{2}{3}} \cdot \sqrt{i_0} = \frac{n \cdot L}{\alpha \cdot K},\tag{A3}$$

The discharge Q can be expressed as:

395
$$Q = \frac{f(H) \cdot R^{\frac{2}{3}}}{n} \cdot \sqrt{i_0}$$
, (A4)

where f(H) is the cross-sectional area as a function of bankfull depth H.

Differentiating Eq. (A4) with respect to *H*:

$$\frac{\partial Q}{\partial H} = \frac{\sqrt{l_0}}{n} \left(f'(H) \cdot R^{\frac{2}{3}} + \frac{2}{3} f(H) \cdot R^{-\frac{1}{3}} \cdot R' \right),\tag{A5}$$

The characteristic river length l is:

$$400 \quad l = \frac{Q}{i_0} \cdot \frac{\partial H}{\partial Q}, \tag{A6}$$

Substituting Eq. (A5) into Eq. (A6):

$$l = \frac{Q}{i_0} \cdot \frac{n}{\sqrt{i_0} \left(f'(H) \cdot R^{\frac{2}{3}} + \frac{2}{3} f(H) \cdot R^{-\frac{1}{3}} \cdot R' \right)},$$
(A7)

From the Muskingum routing method:

$$l = \left(\frac{1}{2} - X\right) \cdot 2L \,, \tag{A8}$$

405 Combining Eqs. (A7) and (A8) gives the expression for slope:





$$i_0 = \frac{f(H)}{\left(\frac{1}{2} - X\right) \cdot 2L \cdot \left(f'(H) + \frac{2}{3} f(H) \cdot R^{-1} \cdot R'\right)},\tag{A9}$$

A.2 Adjustment of Wave-to-Flow Velocity Conversion Coefficient

Using the kinematic wave theory:

$$C = \frac{dQ}{dA} = u \left(1 + \frac{A}{u} \frac{du}{dA} \right) \Rightarrow \alpha = 1 + \frac{A}{u} \frac{du}{dA}, \tag{A10}$$

410 Combining Eq. (A1) and chain rule derivation yields:

$$\alpha = 1 + \frac{2}{3}R', \tag{A11}$$

A.3 Single-Layer CERCX Derivation

A.3.1 Rectangular-shaped CERCX

Assuming the cross-section is rectangular, the hydraulic radius simplifies to $R_r = H_r$, the cross-sectional area $f(H_r) = B_r$.

415
$$H_r$$
, $f'(H_r) = B_r$ and $\alpha_r = \frac{5}{3}$.

Substituting into Eq. (A9) and solving sequentially gives:

$$i_{0r} = \frac{3}{10(\frac{1}{2} - X_l) \cdot L} \cdot H_r , \qquad (A12)$$

$$H_r = \left(\frac{n \cdot L}{\alpha_r \cdot K_L i_{or}}\right)^{\frac{3}{2}},\tag{A13}$$

$$B_r = \frac{n \cdot Q}{\frac{5}{H_r^3} \cdot \sqrt{i_{0r}}},\tag{A14}$$

420 A.3.2 Parabolic-shaped CERCX

When the channel cross-section is approximated as a parabolic shape, the top width is expressed as: $B_p = \beta \sqrt{H_p}$. The cross-sectional area $f(H_p)$ is given as follows:

$$f(H_p) = \int_0^{H_p} B_p dh_p = \frac{2}{3} \beta H_p^{\frac{3}{2}}, \tag{A15}$$

Thus, $f'(H_p) = \beta \sqrt{H_p}$, $R_p = \frac{A_p}{B_p} = \frac{2}{3}H_p$ and $\alpha_p = \frac{13}{9}$. Where β is a coefficient characterizing the parabolic curve.

425 Substituting into Eq. (A9) and solving sequentially gives:

$$i_{0p} = \frac{{}_{13}(\frac{1}{2} - X_I) \cdot L}{{}_{13}(\frac{1}{2} - X_I) \cdot L},\tag{A16}$$





$$H_p = \frac{3}{2} \left(\frac{n \cdot L}{\alpha_p \cdot K_l \cdot \sqrt{i_{0p}}} \right)^{\frac{3}{2}},\tag{A17}$$

$$\beta = \frac{\left(\frac{3}{2}\right)^{\frac{3}{3}} n \cdot Q}{\frac{13}{H_p} \cdot \sqrt{i_{0p}}}, B_p = \beta \sqrt{H_p} , \tag{A18}$$

A.3.3 Triangular-shaped CERCX

When the channel cross-section is approximated as a triangular shape, the top width is expressed as: $B_t = \gamma H_t$, where γ is a coefficient characterizing the triangular shape. Thus, $f(H_t) = 0.5H_t \cdot B_t$, $f'(H_t) = 0.5B_t$, $R_t = 0.5H_t$ and $\alpha_t = \frac{4}{3}$. Substituting into Eq. (A9) and solving sequentially gives:

$$i_{0t} = \frac{{}_{10}H_t}{{}_{10}(\frac{1}{2}-X_t)\cdot L},\tag{A19}$$

$$H_t = 2\left(\frac{n \cdot L}{\alpha_t \cdot K_t \cdot i_{0t}}\right)^{\frac{3}{2}},\tag{A20}$$

435
$$\gamma = \frac{\frac{5}{2\bar{3}n \cdot Q}}{\frac{8}{Hr^{\bar{3}} \cdot \sqrt{i_{0}t}}}, B_{t} = \gamma H_{t}$$
, (A21)

A.4 Dual-Layer CERCX Derivation

A.4.1 General Setup

First layer: known K_{nl1} , X_{nl1} , $Q_1 \Rightarrow B_1$, H_1 , i_0

Second layer: known K_{nl2}, X_{nl2}, Q_2 , unknowns: H_2, a, b

440 Second-layer top width (exponential):

$$B_e = b \cdot H_2^{\ a} + B_1 \,, \tag{A22}$$

$$F(H_2) = \int_0^{H_2} B_e \, dh = \frac{b}{a+1} H_2^{a+1} + B_1 \cdot H_2 + A_1 \,, \tag{A23}$$

$$R'(H_2) = a \cdot b \cdot H_2^{a-1} \,, \tag{A24}$$

A.4.2 Combined Expressions

From Eq. (A3), Eq. (A4), and Eq. (A9), and by substituting hydraulic expressions:

$$F(H_2) = \frac{\alpha_2 \cdot K_{nl_2} \cdot Q_2}{I},\tag{A25}$$





$$B = \frac{i_0^{\frac{3}{4}} \cdot Q_2}{\frac{3}{n^2}} \cdot \left(\frac{\alpha_2 \cdot K_{nl2}}{L}\right)^{\frac{5}{2}},\tag{A26}$$

$$R'(H_2) = \frac{3}{2} \left(\frac{n^{\frac{3}{2} \cdot L^{\frac{1}{2}}}}{i_0^{\frac{7}{4} \cdot (\alpha_2 \cdot K_{nl2})^{\frac{3}{2} \cdot (1 - 2X_{nl2})}}} - 1 \right),\tag{A27}$$

$$\alpha_2 = \left(\frac{n^{\frac{3}{2} \cdot L^{\frac{1}{2}}}}{i_0^{\frac{7}{4} \cdot K_{nl2}} i_0^{\frac{3}{2} \cdot (1 - 2X_{nl2})}}\right)^{\frac{2}{5}},\tag{A28}$$

450 Notation

 Δt time step, s(seconds)

I inflow, m^3/s

O outflow, m³/s

K main parameter of the Muskingum routing method, s(seconds)

455 X main parameter of the Muskingum routing method

 C_0 routing coefficient

 C_1 routing coefficient

 C_2 routing coefficient

l characteristic river length, m

460 L river reach length, m

Q characteristic discharge, m³/s

 k_s , k_0 , x_s , x_0 empirical coefficients of nonlinear Muskingum routing method

 K_l linear parameter of the Muskingum routing method, s(seconds)

 X_l linear parameter of the Muskingum routing method

465 K_{nl1} the main parameter of first-layer's nonlinear Muskingum routing method, s(seconds)

 X_{nl1} the main parameter of first-layer's nonlinear Muskingum routing method

 Q_1 characteristic discharge of first-layer, m³/s

 K_{nl2} the main parameter of second layer's nonlinear Muskingum method, s(seconds)

 X_{nl2} the main parameter of second layer's nonlinear Muskingum method

470 Q_2 characteristic discharge of second layer, m³/s

u flow velocity, m/s

n roughness coefficient

H the bankfull depth, m

R hydraulic radius, m





- 475 R' the derivative of the hydraulic radius function R with respect to H
 - i_0 average slope of the river channel
 - C wave celerity under steady flow conditions, m/s
 - α wave-to-flow velocity conversion coefficient
 - f(H) cross-sectional area as a function of the bankfull depth, m²
- 480 A cross-sectional area, m
 - $\alpha_r, \alpha_p, \alpha_t$ conversion coefficient of rectangular, parabolic and triangular shaped CERCX
 - i_{0r} , i_{0p} , i_{0t} average slope of rectangular, parabolic and triangular shaped CERC
 - R_r , R_p , R_t hydraulic radius of rectangular, parabolic and triangular shaped CERCX, m
 - H_r , H_p , H_t bankfull depth of rectangular, parabolic and triangular shaped CERCX, m
- 485 B_r , B_p , B_t , B_e top width of rectangular, parabolic, triangular and exponential shaped CERCX, m
 - β shape coefficient for a single-layer parabolic-shaped CERCX
 - γ shape coefficient for a single-layer triangular-shaped CERCX
 - B total width of the CERCX, m
 - B_1 top width of the first-layer CERCX, m
- 490 H_1 bankfull depth of the first-layer CERCX, m
 - H_2 bankfull depth of the second-layer CERCX, m
 - $F(H_2)$ the function of the CERCX area with respect to H_2 , m²
 - $F'(H_2)$ the derivative of the CERCX area function with respect to H_2
 - $R'(H_2)$ the derivative of the hydraulic radius function R with respect to H_2
- 495 a cross-sectional shape coefficient of the second layer
 - b cross-sectional shape coefficient of the second layer
 - $Q_{sim}(i)$ simulated discharge at the *i*-th time step, m³/s
 - $Q_{0bs}(i)$ observed discharge at the *i*-th time step, m³/s
 - N the number of data points
- 500 $Q_{0bs\ max}$ the maximum observed discharge, m³/s
 - $Q_{sim\ max}$ the maximum simulated discharge, m³/s





References

- Anees, M.T., Abu Bakar, A.F.B., Khan, M.M.A., Syakir, M.I., Abdullah, K., Nordin, M.N.M., Abdelrahman, K., Eldosouky, A.M., Andráš, P., Bin E.M. Yahaya, N.K., Johar, Z., Mohd Omar, F., Abdul Kadir, M.O., 2022. An alternative approach to estimate river cross-sections using LIDAR-based digital elevation model. Hydrol. Sci. J. 67, 996–1010. https://doi.org/10.1080/02626667.2022.2053129
 - Annayat, W., Sil, B.S., 2020. Assessing channel morphology and prediction of centerline channel migration of the Barak River using geospatial techniques. Bull. Eng. Geol. Environ. 79, 5161–5183. https://doi.org/10.1007/s10064-020-01894-9
- Barbetta, S., Moramarco, T., Perumal, M., 2017. A Muskingum-based methodology for river discharge estimation and rating curve development under significant lateral inflow conditions. J. Hydrol. 554, 216–232. https://doi.org/10.1016/j.jhydrol.2017.09.022
 - Bonakdari, H., Gholami, A., Mosavi, A., Kazemian-Kale-Kale, A., Ebtehaj, I., Azimi, A.H., 2020. A Novel Comprehensive Evaluation Method for Estimating the Bank Profile Shape and Dimensions of Stable Channels Using the Maximum Entropy
- 515 Principle. Entropy 22, 1218. https://doi.org/10.3390/e22111218
 - Casas, A., Benito, G., Thorndycraft, V.R., Rico, M., 2006. The topographic data source of digital terrain models as a key element in the accuracy of hydraulic flood modelling. Earth Surf. Process. Landf. 31, 444–456. https://doi.org/10.1002/esp.1278
- Coletta, V.R., Pagano, A., Zimmermann, N., Davies, M., Butler, A., Fratino, U., Giordano, R., Pluchinotta, I., 2024. Socio-520 hydrological modelling using participatory System Dynamics modelling for enhancing urban flood resilience through Blue-
 - Green Infrastructure. J. Hydrol. 636, 131248. https://doi.org/10.1016/j.jhydrol.2024.131248

 Cunge, J.A., 1969. On The Subject Of A Flood Propagation Computation Method (MuskIngum Method). J. Hydraul. Res. 7,
 - 205–230. https://doi.org/10.1080/00221686909500264

 He H., Zhang J., 1998. A New Mathematical Algorithmfor Estimating the Parameters of the Muskingum River Flow Routing
- 525 Model. J. China Hydrol. 15–18. https://doi.org/10.19797/j.cnki.1000-0852.1998.05.003
 - Horritt, M.S., Bates, P.D., 2002. Evaluation of 1D and 2D Numerical Models for Predicting River Flood Inundation. J. Hydrol. 268, 87–99. https://doi.org/10.1016/S0022-1694(02)00121-X
 - Ike, C.C., 2024. Galerkin-Kantorovich variational method for solving saint venant torsion problems of rectangular bars. J. Mech. Eng. Autom. Control Syst. 05, 10–22. https://doi.org/10.21595/jmeacs.2024.23928
- Intergovernmental Panel on Climate Change (IPCC), 2023. Climate change 2021 the physical science basis: Working group I contribution to the sixth assessment report of the intergovernmental panel on climate change. Cambridge University Press, Cambridge. https://doi.org/10.1017/9781009157896
 - Kiesel, J., Wolff, C., Lorenz, M., 2024. Brief communication: From modelling to reality flood modelling gaps highlighted by a recent severe storm surge event along the German Baltic Sea coast. Nat. Hazards Earth Syst. Sci. 24, 3841–3849.
- 535 https://doi.org/10.5194/nhess-24-3841-2024





- Liu, H., Wang, H., Liu, S., Hu, C., Ding, Y., Zhang, J., 2015. Lattice Boltzmann method for the Saint-Venant equations. J. Hydrol. 524. https://doi.org/10.1016/j.jhydrol.2015.03.002
- McCarthy, G.T., 1939. The Unit Hydrograph and Flood Routing. Army Engineer District, Providence.
- Niu C., Li D., Zhao L., Han S., Quan L., Li Y., Hu C., 2024. Evolution of Channel Roughness and Influencing Factors in the
- 540 Wide Floodplain of the Lower Yellow River in Recent 20 Years. J. Basic Sci. Eng. 32, 984–999 https://doi.org/10.16058/j.issn.1005-0930.2024.04.006
 - Nurbatsina, A., Salavatova, Z., Tursunova, A., Didovets, I., Huthoff, F., Rodrigo-Clavero, M.-E., Rodrigo-Ilarri, J., 2025. Flood modelling of the Zhabay river basin under climate change conditions. Hydrology 12, 35. https://doi.org/10.3390/hydrology12020035
- Pfahl, S., O'Gorman, P.A., Fischer, E.M., 2017. Understanding the regional pattern of projected future changes in extreme precipitation. Nat. Clim. Change 7. https://doi.org/10.1038/nclimate3287
 - Rui, X., Liu, F., Yu, M., 2008. Discussion of Muskingum method parameter X. Water Sci. Eng. 1, 16–23. https://doi.org/10.3882/j.issn.1674-2370.2008.03.002
 - Salvati, A., Moghaddam Nia, A., Salajegheh, A., Moradi, P., Batmani, Y., Najafi, S., Shirzadi, A., Shahabi, H., Sheikh-Akbari,
- A., Jun, C., Clague, J.J., 2023. Performance improvement of the linear muskingum flood routing model using optimization algorithms and data assimilation approaches. Nat. Hazards 118, 2657–2690. https://doi.org/10.1007/s11069-023-06113-8 Salvati, A., Moghaddam Nia, A., Salajegheh, A., Shirzadi, A., Shahabi, H., Ahmadisharaf, E., Han, D., Clague, J.J., 2024. A
 - Satyaprasad, D., Kuiry, S.N., Sundar, S., 2023. A shock-capturing meshless method for solving the one-dimensional saint-

systematic review of Muskingum flood routing techniques. Hydrol. Sci. J. 69, 810-831.

venant equations on a highly variable topography. J. Hydroinformatics 25, 1235–1255. https://doi.org/10.2166/hydro.2023.164 Zhang, X., Zhengzheng, B., Sun, X., Wang, P., Xu, Z., Jia, B., 2023. Backwater Effects in Rivers and Lakes: Case Study of Dongping Lake in China. Water 15, 3850. https://doi.org/10.3390/w15213850